

FABRICATION OF NANO CLAY INTERCALATED POLYMERIC MICROBEADS FOR CONTROLLED RELEASE OF CURCUMIN

DHARMENDER PALLERLA^a, SUMAN BANOTH^b, SUNKARI JYOTHI^{a*}

^{a,b}Department of Chemistry, Kakatiya University, Warangal 506009 Telangana, India
Email: jyothisri97@yahoo.co.in

Received: 09 Oct 2020, Revised and Accepted: 28 Nov 2020

ABSTRACT

Objective: The objective of this study was to formulate and evaluate the Curcumin (CUR) encapsulated sodium alginate (SA)/badam gum (BG)/kaolin (KA) microbeads for controlled drug release studies.

Methods: The fabricated microbeads were characterized by fourier transform infrared spectroscopy (FTIR), differential scanning calorimetry (DSC), thermogravimetric analysis (TGA), X-ray diffraction (X-RD), and scanning electron microscopy (SEM). Dynamic swelling studies and *in vitro* release kinetics were performed in simulated intestinal fluid (pH 7.4) and simulated gastric fluid (pH 1.2) at 37 °C.

Results: FTIR confirms the formation of microbeads. DSC studies confirm the polymorphism of CUR in drug loaded microbeads which indicate the molecular level dispersion of the drug in the microbeads. SEM studies confirmed the microbeads are spherical in shape with wrinkled and rough surfaces. XRD studies reveal the molecular dispersion of CUR and the presence of KA in the developed microbeads. *In vitro* release studies and swelling studies depend on the pH of test media, which might be suitable for intestinal drug delivery. The % of drug release values fit into the Korsmeyer-Peppas equation and n values are obtained in the range of 0.577-0.664, which indicates that the developed microbeads follow the non-Fickian diffusion drug release mechanism.

Conclusion: The results concluded that the CUR encapsulated microbeads are potentially good carriers for controlled drug release studies.

Keywords: Sodium alginate, Badam Gum, Kaolin, Curcumin, Microbeads, Drug delivery

© 2021 The Authors. Published by Innovare Academic Sciences Pvt Ltd. This is an open access article under the CC BY license (<http://creativecommons.org/licenses/by/4.0/>)
DOI: <http://dx.doi.org/10.22159/ijap.2021v13i1.39965>. Journal homepage: <https://innovareacademics.in/journals/index.php/ijap>

INTRODUCTION

A drug delivery system is designed to allow a therapeutic agent to be introduced into the biological organism and to enhance its effectiveness and safety by controlling the release rate, time and place of drug release in the body [1]. The development of effective therapeutic drug delivery systems is essential for medicine and health care in order to increase the safety, efficacy, and bioavailability of the drugs. Over the past few decades, polymeric matrices are used in many pharmaceutical applications because it offers various advantages like efficiency in administering the drug to the specific target at a proper time thereby improving the overall therapeutic response of a dosage form, high water absorption tendency and capable of swelling under physiological conditions [2-4]. Hence, the utility of polymeric materials is increasing day by day as the pharmaceutical industry expands globally. Now-a-days, Polymeric interpenetrating polymer network hydrogels have been widely used in biomedical applications such as drug delivery and tissue engineering due to their water intake capacity, biocompatibility, and biodegradability [5]. However, IPN hydrogels dosage forms have few drawbacks like uncontrolled swelling and release rate, which leads to several side effects. The polymeric networks are crosslinked with several crosslinking agents, coated with other polymers and intercalated with clay minerals, which control the release and swelling rates. Presence of clay minerals in polymeric matrices, minimizing side effects and maintaining the effective drug concentration in plasma over a period of time [6].

From the last few decades, clay minerals are used in solid and semisolid pharmaceutical preparations for topical and oral administration, as well as cosmetic formulations [7, 8]. Kaolin is a hydrated two-dimensional (2D) aluminosilicate clay mineral, used as active ingredients due to their uninjured bioactivity and therapeutic effects. They are developed as a hemostatic agent, dermatological protector, anti-inflammatory agent and pelotherapy, or oral products as a gastrointestinal protector, antimicrobial, detoxifying or anti-diarrheal agent in health-care topical items [9-13]. Moreover, kaolin and its modified derivatives have recently been considered a

promising material in many areas of biomedical research, such as drug, protein and gene delivery, based on the high capacity of interaction with organic and biochemical molecules, bio-adhesion and cellular uptake. It can acts as an active ingredient or as adjuvant component in pharmaceutical dosage forms by controlling the efficiency and consistency in the dosage formulations and improving the drug bioavailability [14-16].

Sodium alginate (SA) is a linear polymer that has D-mannuronic acid and L-guluronic acid residues in the polymer chain, obtained from brown seaweed [17]. SA is one of the most adaptable, versatile polymers, widely used in the food, cosmetic, and pharmaceutical industries because of its properties like biocompatible, biodegradable, inherent hydrophilicity, non-toxic and good potentiality in drug delivery applications [18]. In recent decades, it is used as a potential tool for developing a different type of controlled, sustained, and targeted drug delivery systems. In addition, it is also used in the semisolid formulation and wound dressing applications [19]. Badam gum (BG) is a natural gum obtained from *Terminalia catappa* LINN, belongs to the family Combretaceae [20]. It can be used in pharmaceutical applications because of its abundant availability, reliability, efficiency, eco-friendly, and economical features. Previously Srikanth *et al.* [21] has reported that BG was used in controlled drug delivery systems as a retarding polymer for a highly soluble drug like propranolol HCl.

Curcumin is a natural bioactive compound derived from the *Curcuma longa* species and possesses a wide range of pharmacological properties such as antifungal, antiviral, antibacterial, anti-inflammatory, anti-malarial, antioxidant, anti-mutagenic agent, wound healing properties as well as it enhances anti-tumour activity against different types of cancer cells [22-24]. However, due to its poor water-solubility, short life and low bioavailability, the therapeutic use of CUR are limited [25, 26]. Generally, simple ionotropic gelation techniques are used to encapsulate hydrophilic drugs in hydrogel beads, but because of its poor water solubility, this technique gives low CUR encapsulation efficiency. Thus, in the present study, KA clay material was used to increase the drug encapsulation efficiency of CUR, the

muco-adhesiveness of KA clay material facilitates the intercalation of drug molecules which in turn increases the encapsulation and bioavailability of CUR.

In the present research work, we focussed on the fabrication of nano KA clay intercalated with SA/BG microbeads. The presence of KA in the polymer networks increases the bioavailability of CUR and also controls the release rate of CUR. The developed microbeads were characterized by different techniques such as FTIR, DSC, TGA, X-RD, and SEM. The swelling studies and *in vitro* drug release kinetics were performed in both simulated intestinal fluid and simulated gastric fluid at 37 °C and the results are presented here.

MATERIALS AND METHODS

Materials

Badam gum and Kaolin were purchased from Sigma Aldrich (USA). Sodium alginate and calcium chloride were purchased from Sd. Fine chemicals, Mumbai, India. Curcumin was purchased from Loba Chemicals, Mumbai, India. Double distilled water was used throughout the study.

Methods

Preparation of SA/BG/KA microbeads

A Simple gelation method was used to fabricate drug-loaded SA/BG/KA microbeads [7]. Briefly, different amounts of SA and BG (table 1) were dissolved in water overnight under constant stirring. Different blends of these solutions were prepared by mixing varying amounts of SA and BG



Scheme 1: Schematic procedure for the preparation of CUR encapsulated SA/BG/KA microbeads

Table 1: Formulation and composition of all samples

| Formulation code | SA (mg) | BG (mg) | Water (ml) | KA (mg) | Drug (mg) |
|------------------|---------|---------|------------|---------|-----------|
| SB1 | 320 | 80 | 20 | 100 | 100 |
| SB2 | 280 | 120 | 20 | 100 | 100 |
| SB3 | 240 | 160 | 20 | 100 | 100 |
| SB4 | 240 | 160 | 20 | 200 | 100 |
| SB5 | 240 | 160 | 20 | 300 | 100 |
| SB6 | 240 | 160 | 20 | 100 | 150 |
| SB7 | 240 | 160 | 20 | 100 | 200 |
| Placebo | 240 | 160 | 20 | 00 | 000 |

Thermal analysis

To investigate the molecular dispersion of CUR and thermal stability of KA intercalated SA/BG/CUR loaded microbeads, differential scanning calorimetry (DSC) and Thermogravimetric analysis (TGA) were performed by heating the sample at a heating rate of 10 °C/min under nitrogen atmosphere from 40 to 600 °C.

X-ray diffraction (XRD)

The X-ray diffraction of CUR, KA, placebo microbeads, and drug loaded microbeads were performed by a wide angle X-ray scattering diffractometer (Panalytical X-ray Diffractometer, model-X'pert Pro) with CuK α radiation ($\lambda = 1.54060$) at a scanning rate of 10 °/min to determine the crystallinity.

Scanning electron microscopy (SEM)

The morphological characterization of microbeads was observed by using SEM (JOEL MODEL JSM 840A) with an accelerated voltage of 20 kV.

Encapsulation efficiency

The encapsulation efficiency of drug loaded microbeads was estimated by the following procedure. Weight exactly 20 mg of

(as per given in table 1) and stirred well until to obtain a complete homogeneous solution. To this blend solution, different amounts of CUR and KA (table 1) were added and stirred well up to the formation of a homogeneous mixture. Then the blend mixture was added drop wise into 5% CaCl₂ solution through a syringe (1 mm diameter) under constant stirring. The obtained microbeads were collected by decantation, washed three times with double distilled water to remove the drug attached on the bead surface, and finally were dried in air overnight at room temperature. A schematic diagram (Scheme 1) for the synthesis of CUR encapsulated SA/BG/KA microbeads was given below

Characterizations methods

Intercalation kinetics

The intercalation time of CUR with KA was estimated by the following procedure. Briefly, 50 mg of CUR and 100 mg of KA was weighed and dissolved in 20 ml of double distilled water with continuous stirring at 37 °C. At regular intervals of time, the drug solution was filtered and concentration of CUR was assayed using UV spectrophotometer at fixed λ_{max} value of 470.00 nm.

Fourier transform infrared (FTIR) spectral analysis

To find out the type of bonding as well as the ionic interactions between polymers, KA and CUR fourier transform infrared spectroscopy spectra were performed and the developed microbeads were recorded with FTIR spectrophotometer (model Bomem MB-3000, with Horizon MBTM FTIR software) in the wavelength range of 400–4000 cm⁻¹.

microbeads and placed into 100 ml of phosphate buffer solution (pH 7.4 containing 5 % absolute ethyl alcohol) for 24 h. Afterward, the solution was stirred and placed sonication for 5 min to ensure the complete extraction of CUR from the microbeads. Supernatants were filtered and analyzed by ultraviolet (UV) spectrophotometer (LabIndia, Mumbai, India) at the λ_{max} of 470.00 nm with placebo microbeads were used as a blank correction. The percentage of encapsulation efficiency was determined by the following formula.

$$\% EE = \frac{W_i}{W_i} \times 100$$

Where W_i is total amount of CUR in the microbeads and W_i is total amount of CUR initially added during the preparation

Swelling measurements

The swelling behaviour of different formulations was determined gravimetrically in simulated intestinal fluid (pH 7.4) and simulated gastric fluid (pH 1.2) at 37 °C. The % of equilibrium swelling degree was calculated using the following equation:

$$\% \text{ swelling degree} = \frac{W_w - W_d}{W_d} \times 100$$

Where W_w is the weight of the wet microbeads and W_d the weight of the dried microbeads.

In vitro drug release studies

In vitro drug release studies of developed microbeads were carried out in simulated intestinal fluid (pH 7.4) and simulated gastric fluid (pH 1.2) at 37 °C using a dissolution tester (Lab India, Mumbai, India). Briefly, 100 mg of drug loaded microbeads were taken in a dialysis bags and placed in 900 ml of phosphate buffer solution (PBS) at a rotation speed of 50 rpm. At regular intervals of time, 5 ml aliquot samples were withdrawn, and analyzed using UV spectrophotometer at fixed λ_{max} value of 470.00 nm, at the same time equal amount of PBS sample was added into the system to maintain sink condition.

Drug release kinetics

The drug release kinetics was analyzed by fitting the data into kinetic models, which include zeroth, first order, Higuchi and Korsmeyer-Peppas [27-30]. Based on the goodness of data fit, the most suitable model was also determined [31].

RESULTS AND DISCUSSION

Intercalation kinetics

To investigate the intercalation time of CUR with KA intercalation kinetics were performed and the result was displayed in fig. 1. The result reveals that 14.59 % of CUR intercalated with electrostatically within 90 min and remained constant up to 360 min. Therefore in the present study, we should maintain 90 min time for interaction between CUR and KA to prevent partial interaction.

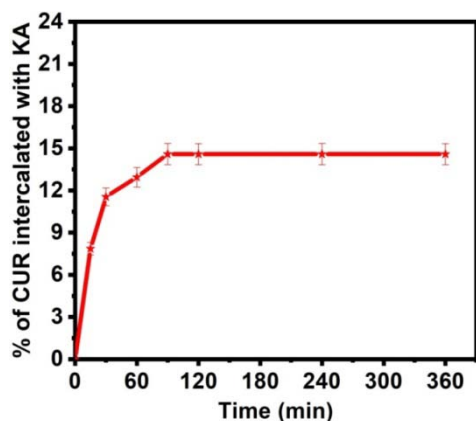


Fig. 1: Effect of time for intercalation of CUR with KA

FTIR spectral analysis

To find out the type of bonding as well as the ionic interactions between polymer, CUR and KA FTIR analysis were performed and the results are displayed in fig. 2. The FTIR spectra of CUR show characteristic bands at 3496 cm^{-1} and 2923 cm^{-1} , which corresponds to phenolic O-H stretching and aromatic C-H stretching vibrations respectively, a band at 1513 cm^{-1} corresponds to mixed (C=O) and (C=C) vibration, a band at 1272 cm^{-1} is assigned to Ar-O stretching vibrations [25]. The absorption bands of KA which were found at 3688, 3625, 3456 and 2360 cm^{-1} can be associated with the O-H, Si/Al-OH, H-O-H and C-H stretching frequencies respectively, the absorption bands at 1126 and 902 cm^{-1} corresponds to Si-O-Si stretching band [32]. The FTIR spectra of SA show bands at 3417, 1596 and 1383 cm^{-1} may be attributed to symmetric and asymmetric stretching frequencies of hydroxyl (O-H), carbonyl (C=O) and carboxylate (COO-) groups respectively. On comparing the FTIR spectra of placebo microbeads and drug loaded microbeads (SB7), a new band at 1575 cm^{-1} was observed, which similar to that of Ar-O stretching vibration of CUR, suggesting that drug was present in SB7. And also the band at 1594 cm^{-1} in placebo microbeads was shifted to 1588 cm^{-1} in drug loaded SB7 microbeads, which confirmed that the drug interacts with the polymer matrix. In case of SB7 the O-H stretching frequency was decreased due to the intermolecular hydrogen bonding between silanol groups on the clay surface and the

hydroxyl or carboxyl groups of polymer molecules and also a new band appears at 911 cm^{-1} , which confirmed that the KA intercalates with active sites of polymer matrices and drug molecules [33].

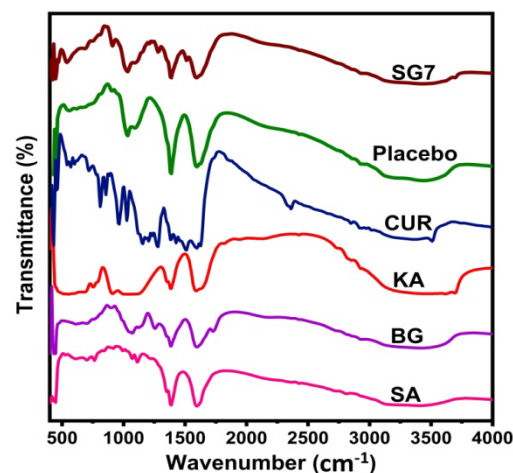


Fig. 2: FTIR spectra of SA, BG, KA, CUR, placebo microbeads, and drug loaded microbeads (SB7)

Thermal analysis

To investigate the crystalline nature of CUR in the polymer matrix as well as the interaction of KA with polymer matrix DSC analysis was performed and the results were displayed in fig. 3. The DSC of KA showed peaks at 272 and 496 °C, whereas SB7 microbeads also showed similar peaks like that of KA at 321 and 481 °C but a slight variation was observed, which confirmed that the interaction takes place between active sites of the polymer matrix and KA. The DSC curve of CUR showed a sharp peak at 189 °C, whereas such a peak was not observed in SB7 microbeads, suggesting that the CUR has molecularly dispersed in the polymer networks.

To find out the thermal stability of microbeads, TGA analysis was performed and the results are shown in fig. 4. The TGA curve of SA showed three weight loss steps, the first weight loss step with weight loss of 17 % was observed in the region of 40–118 °C due to the dehydration process. The next two weight loss steps were found in the region of 123–215 and 227–600 °C with weight loss of 4 and 48 % respectively, which is due to the formation of sodium carbonate residue [34]. The thermal decomposition BG occurs in two steps, the first weight loss step was found in the region of 40–196 °C with a weight loss of 18%, which is due to dehydration of adsorbed water molecules on the surface. The next weight loss step was found in the region of 201–600 °C with a weight loss of 55%, corresponds to the decomposition of BG polymer. The TGA curve of CUR showed that the CUR could remain stable up to 168 °C, following the mass loss and maximum at 391 °C due to the complete degradation of CUR [35]. The thermal decomposition of KA showed two weight loss steps, the first step was observed in the region of 40–256 °C with a loss of 6 % followed by weight loss of 13% in the region of 259–600 °C, corresponds to the loss of structural water molecules [7]. The TGA curve of placebo microbeads showed three consecutive weight loss steps, the first weight loss step with a loss of 24 % was found in between 40–192 °C, which corresponds to dehydration of adsorbed water molecules. The second step was observed in the region of 197–305 °C with a loss of 34% followed by the weight loss of 8% was observed in the region of 311–600 °C, due to the decomposition of the polymer network. Similarly, CUR loaded microbeads (SB7) also showed three weight loss steps, the first weight loss step was found in the region of 40–185 °C with a loss of 15%, that is ascribed to the dehydration of water molecules adsorbed on the surface of microbeads. The next two steps were observed in the region of 191–308 °C and 311–600 °C with a loss of 19 and 14 %, which corresponds to the degradation of the polymer matrix. The TGA results suggest that the developed microbeads show an overall improvement in thermal stability.

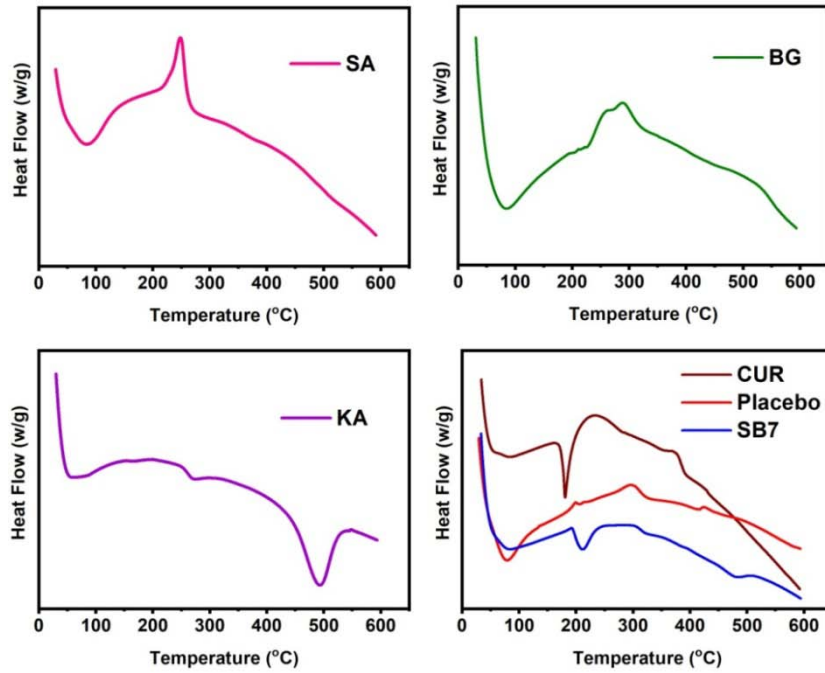


Fig. 3: DSC curves of SA, BG, KA, CUR, Placebo and drug loaded microbeads (SB7)

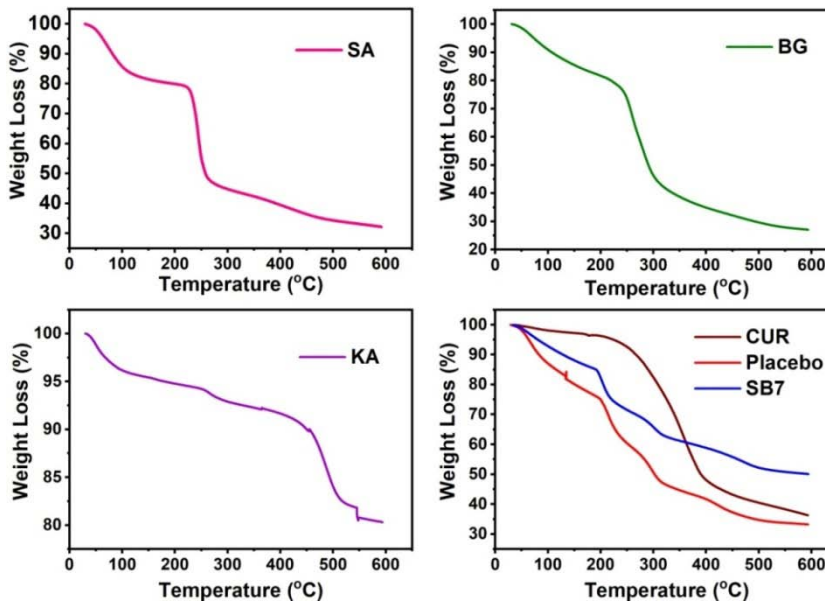


Fig. 4: TGA curves of SA, BG, KA, CUR, Placebo and drug loaded microbeads (SB7)

X-RD analysis

To examine the molecular dispersion of CUR and the presence of KA in the developed microbeads X-RD analysis was performed and the results are displayed in fig. 5. The diffractogram of CUR shows characteristic peaks in the 2θ region of 12-28° because of its crystallinity. These peaks are not observed in the polymer matrix of SB-7 microbeads, which indicates that CUR has molecularly dispersed in the polymeric microbeads. Kaolinite and quartz phases were observed in the kaolin clay. The diffractogram of KA shows characteristic peaks at 11.95°, 18.34°, 19.97° and 24.84° which indicate the presence of kaolinite. A small reflection at 26.6° was observed in the diffractogram of KA, which indicates the presence of traces of quartz. These results are in good agreement with Khan *et al.* [36] who found the same results from the pyrolysis kinetics of the conversion of Malaysian kaolin to metakaolin.

The diffractogram of SB-7 microbeads also showed similar peaks to that of KA with slight variations, suggesting that the KA has successfully loaded in the microbeads.

SEM analysis

The topographical images of developed microbeads were found out using SEM analysis and the images are presented in fig. 6. The microbeads are spherical in shape with wrinkled and rough surfaces. It is interesting that the surface of SB-7 has high roughness compare to placebo microbeads, which indicates the presence of KA platelets on the outer surface of microbeads. A similar observation was reported by Reddy *et al.* [7] from the development of sodium alginate/gelatin microbeads-intercalated with kaolin nanoclay. The average diameter of the microbeads obtained from the SEM was in the range of 700-1300 μm .

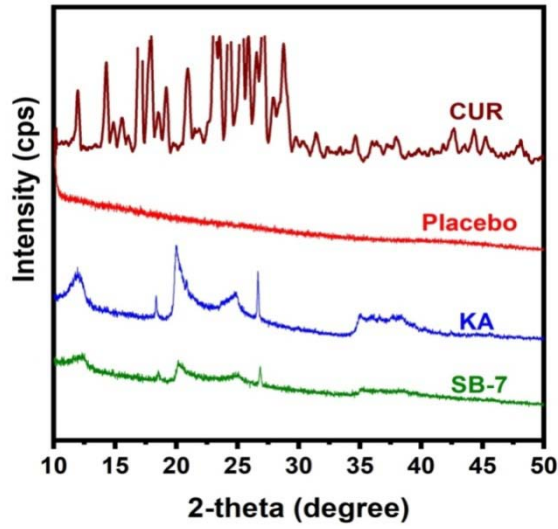


Fig. 5: XRD patterns of CUR, placebo, KA and SB-7

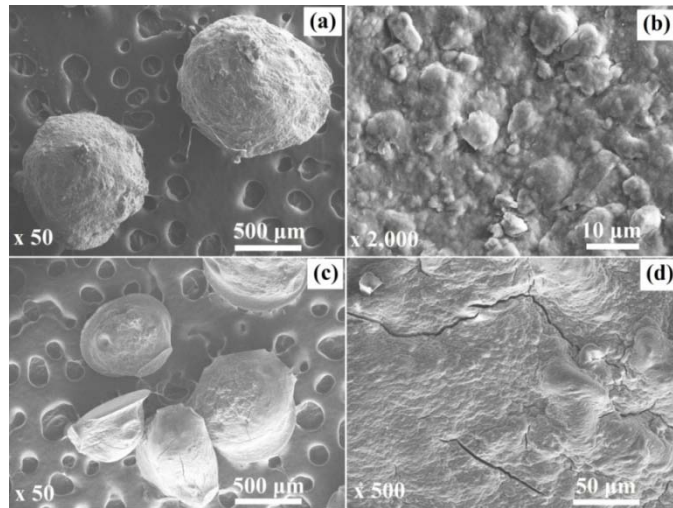


Fig. 6: The topographical images of drug loaded microbeads (SB7) (a and b) and placebo microbeads (c and d)

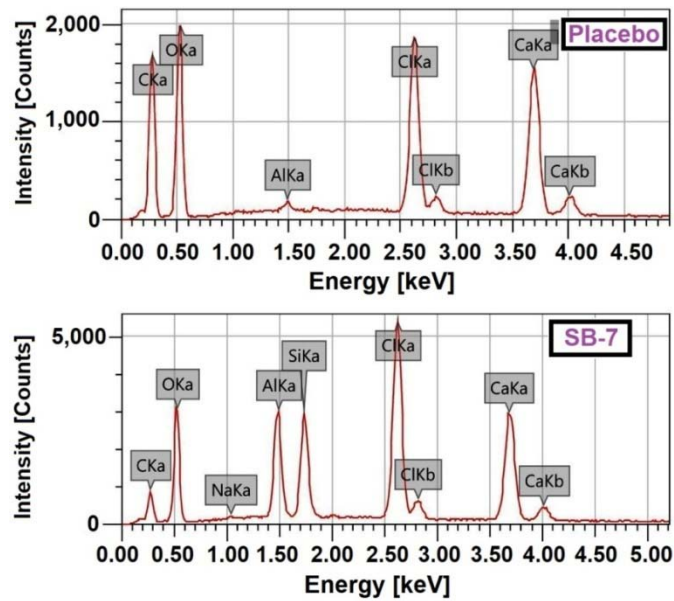


Fig. 7: EDS spectra of placebo and SB-7 microbeads

Energy-dispersive X-ray spectra (EDS) analysis

To find out the elements present in the developed microbeads energy-dispersive X-ray spectra (EDS) analysis were performed and the results are presented in fig. 7. The EDS spectra of placebo microbeads showed C, O, Al, Cl and Ca elemental peaks. Whereas in the case of KA loaded microbeads (SB-7) showed similar elements that of placebo microbeads along with that new elemental peaks such as Na, Si and Al were observed with high intensity, which confirms the presence of KA in the SB-7 microbeads.

Swelling measurements

Swelling degree plays a key role in the controlled release of drugs in polymeric drug delivery systems. In the present study swelling experiments were carried out at pH 1.2 and 7.4 at 37 °C and the results were displayed in fig. 8. From the results, it was clearly observed that a higher swelling degree was observed at pH 7.4 than at pH 1.2, this may be due to at pH 7.4, carboxylic groups show fewer interactions with buffer media and thus the network becomes looser, making it easier for the entrapped drug molecules to leach out of the polymer network. A similar observation was reported by Reddy *et al.* [37] from their glycopyrrolate release studies of sodium

alginate/poly (vinylpyrrolidone-co-vinyl acetate) microbeads. The developed microbeads are therefore good promising carriers for delivering drug molecules to the intestine and preventing the gastric release of drugs.

Encapsulation efficiency (% EE)

The percentages of encapsulation efficiency (% EE) of CUR loaded microbeads are displayed in table 2. The % EE values lies between 45% to 53%. This indicates the %EE dependence on formulation parameters which include % drug loading, polymer blend composition and amount of KA. The % EE increases with the increase of drug loading in the polymer matrix. The % EE increases with an increase of SA in the polymer matrix this is due to curcumin alginate interactions (Hydrophilic and Hydrophobic). A similar observation was observed by Govindaraju *et al.* [38] from their curcumin encapsulated in alginate-polysorbate 80 nanoparticles. The % EE increases with the increase of KA content in the polymer matrix, which is due to the availability of large basal space, good absorption capacity and availability of free-OH groups of KA. The presence of-OH groups develops a hydrogen bonding between CUR and KA, consequently % EE increases.

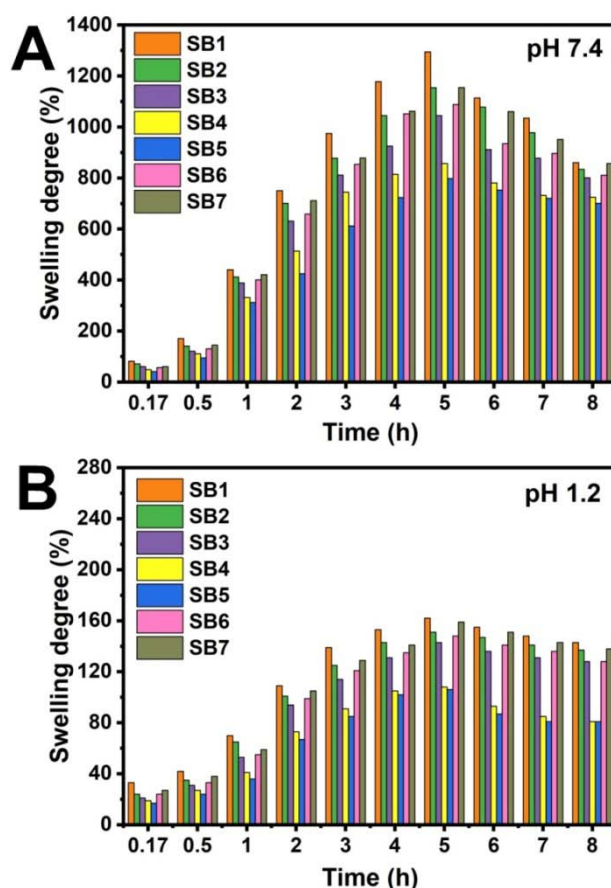


Fig. 8: Swelling studies of all profiles at pH 7.4 and pH 1.2 at 37 °C

Table 2: Encapsulation efficiency (% EE) of all samples

| S. No. | Formulation code | %EE |
|--------|------------------|--------|
| 1 | SB1 | 48±1.6 |
| 2 | SB2 | 47±1.2 |
| 3 | SB3 | 45±0.8 |
| 4 | SB4 | 51±1.3 |
| 5 | SB5 | 53±1.1 |
| 6 | SB6 | 47±1.5 |
| 7 | SB7 | 48±2.1 |

(Results are expressed as mean±SD, n=3)

In vitro drug release studies

The *in vitro* release studies of all profiles were investigated under both pH 1.2 and pH 7.4 at 37 °C and the results are shown in fig. 9 to 12. The findings show that the percentage of CUR release is higher at pH 7.4 than at pH 1.2, which is attributed to at pH 7.4 the carboxylate group has fewer interactions with the buffer media, thus

the network becomes slacker, hence the trapped drug molecules are quickly leached out of the polymer matrix. It has been observed that similar to swelling behaviour, *in vitro* release rate also shows the same type of results. *In vitro* drug release studies for all profiles at pH 7.4 were discussed in terms of polymer blend variation, drug variation, and KA variation, and the results are displayed in fig. 10 to 12.

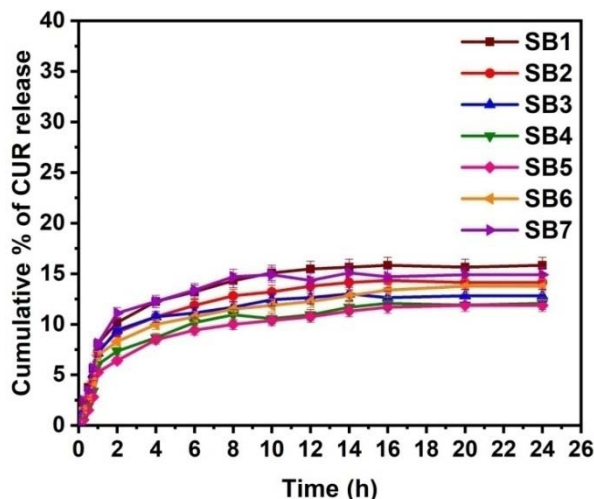


Fig. 9: *In vitro* release profiles of CUR microbeads in PBS pH 1.2 at 37 °C

Effect of polymer content

The effect of the polymer blend matrix on drug release profiles was studied at the constant loading of the drug (100 mg) and KA (100 mg). The drug release profiles of SB1, SB2 and SB3 are 82, 80 and 75 %

respectively are displayed in fig. 10. The percentage of CUR release was increased with the increasing amount of SA, this is due to the more hydrophilic nature of SA. These results are in good agreement with Rao *et al.* [39] who observed similar results from their drug release studies of sodium alginate–locust bean gum IPN hydrogel beads.

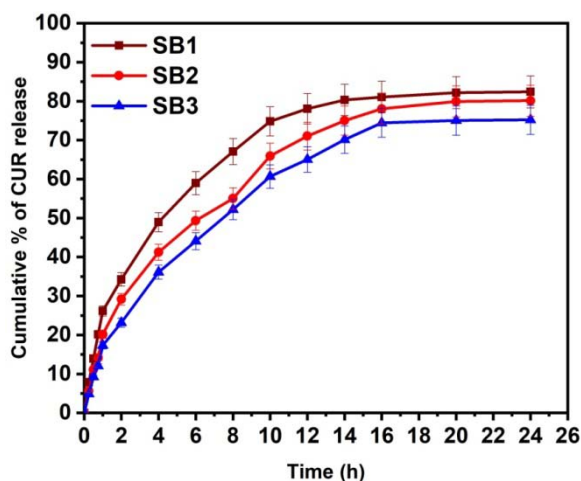


Fig. 10: Effect of polymer blend composition on % of CUR release in PBS pH-7.4 at 37 °C

Effect of KA content

To find out the effect of KA on *in vitro* release profiles were studied at constant polymer matrix and drug content. The release profiles of SB3, SB4 and SB5 are 75, 71 and 66 % respectively are shown in fig. 11. The release rate of CUR was decreased with increasing the KA content, because the intercalated drug molecules cannot be exchanged completely with phosphate ions in the buffer solution during the ion exchange process, which results the incomplete release process, consequently release rate decreases.

Effect of drug content

The effect of drug content on *in vitro* release profiles was studied at the constant polymer and KA content. The release rate of B3 (100 mg), SB6 (150 mg) and SB7 (200 mg) are 75, 77 and 80% respectively are displayed in fig. 12. The results suggesting that as the amount of drug content increases the release rate also increases. Hence, the release rate is higher for those formulations having a higher amount of drug and vice-versa. These results are good agreement with Madhavi *et al.* [40] who found that the drug release rate increases with the increase of drug concentration from their drug release studies of simvastatin.

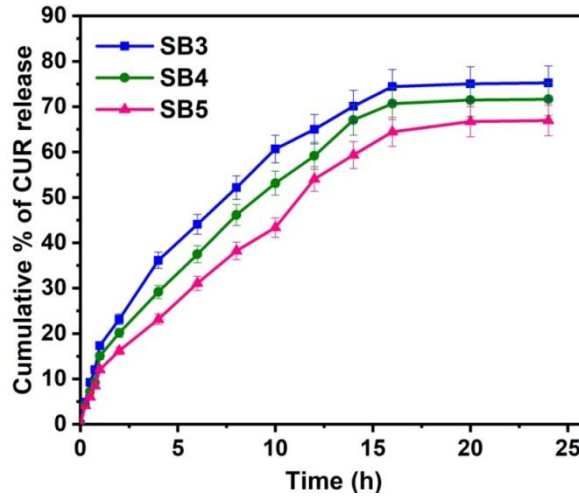


Fig. 11: Effect of KA content on % of CUR release in PBS pH-7.4 at 37 °C

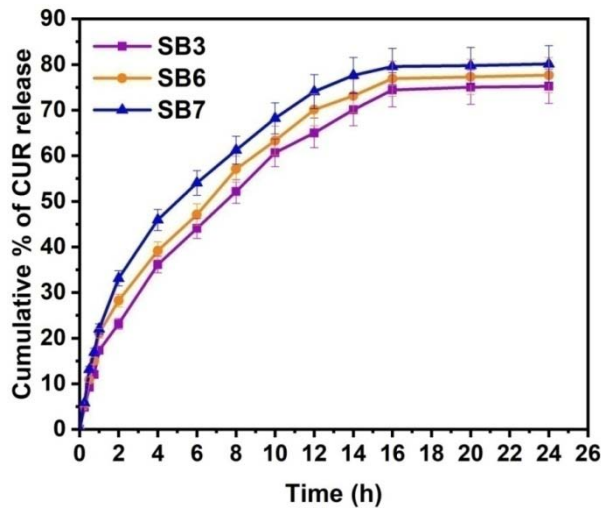


Fig. 12: Effect of drug content on % of CUR release in PBS pH-7.4 at 37 °C

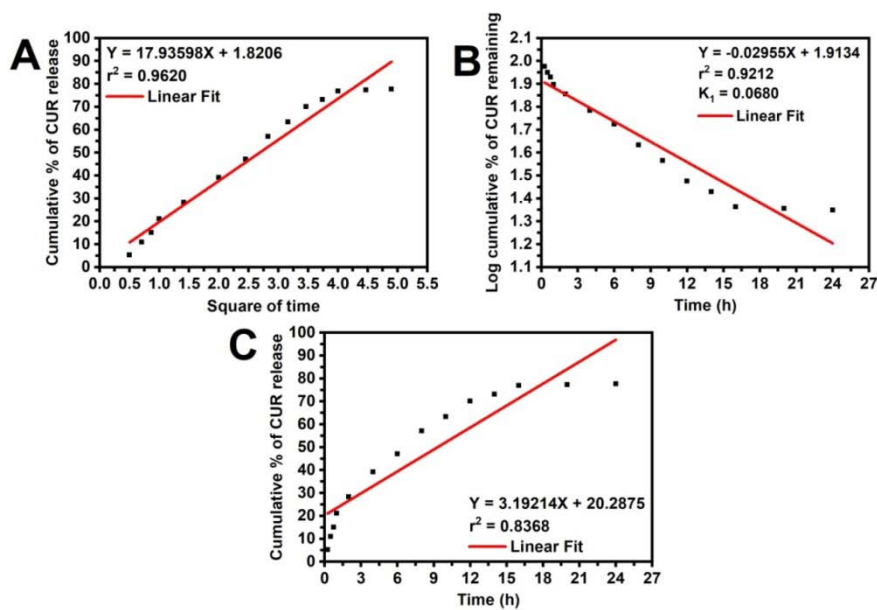


Fig. 13: Evaluation of drug release models in PBS 7.4 at 37 °C (A) Higuchi model (B) first order and (C) zero order

Table 3: Release kinetics parameters at pH-7.4 and encapsulation efficiency (% EE) of all samples

| Formulation code | Korsmeyer peppas | | Higuchi | | First | | Zero | |
|------------------|------------------|-------|----------------|----------------|----------------|----------------|----------------|----------------|
| | r ² | n | r ² | K _H | r ² | K ₁ | r ² | K ₀ |
| SB1 | 0.973 | 0.577 | 0.937 | 18.380 | 0.936 | 0.0780 | 0.768 | 3.201 |
| SB2 | 0.975 | 0.626 | 0.965 | 18.508 | 0.941 | 0.0732 | 0.842 | 3.299 |
| SB3 | 0.985 | 0.650 | 0.970 | 17.831 | 0.947 | 0.0642 | 0.856 | 3.195 |
| SB4 | 0.985 | 0.664 | 0.977 | 17.280 | 0.945 | 0.0588 | 0.888 | 3.138 |
| SB5 | 0.991 | 0.632 | 0.979 | 16.037 | 0.956 | 0.0511 | 0.929 | 2.961 |
| SB6 | 0.964 | 0.623 | 0.962 | 17.935 | 0.921 | 0.0680 | 0.836 | 3.192 |
| SB7 | 0.961 | 0.616 | 0.944 | 18.225 | 0.929 | 0.0731 | 0.813 | 3.201 |

Drug release kinetics

The cumulative drug release data of all profiles were fitted into various mathematical models such as zero order, first order and Higuchi. The correlation coefficient and rate constant values of all models are shown in table 3 and fig. 13. The correlation coefficient values of CUR loaded microbeads were close to the Higuchi model. According to the Higuchi model, the release of drug from the microbeads involves the penetration of liquid into the matrix and dissolves the drug, which then diffuses the drug through pores or intestinal channels into the exterior liquid. However, this type of phenomenon is observed in the hydrophilic matrix system. Therefore the drug release rate of CUR loaded microbeads shows the phenomenon of swelling and erosion of the polymer simultaneously. To understand the drug release mechanism, the *in vitro* release data were fitted into the following Korsmeyer-Peppas equation.

$$\frac{M_t}{M_\infty} = kt^n$$

Where, M_t is the cumulative release of CUR at time t , M_∞ is the total amount of CUR in the matrix, k is a characteristic release constant of the drug-polymer system and n is the release exponent indicating the type of drug release mechanism. The results n and k are listed in table 2. For spherical drug carriers, if $n < 0.43$, the drug diffuses from the polymer matrix according to Fickian diffusion; if $0.43 < n < 0.85$, anomalous or non-Fickian type drug diffusion occurs; if $n = 0.85$, Case-II kinetics is operative; if $n > 0.85$, the mode of drug release follows the super Case-II diffusion. In the present data n values are obtained in the range of 0.577-0.664 indicates non-Fickian type of diffusion process.

CONCLUSION

In the present work, KA intercalated SA/BG microbeads were fabricated using a simple ionotropic gelation method for the controlled release of CUR. FTIR confirmed the interaction between CUR molecules and the polymer network. TGA, DSC and XRD studies confirmed the chemical stability and molecular dispersion of CUR. SEM studies reveal that the developed microbeads are spherical and also the outer surface of SB-7 microbeads showed high roughness which confirms the presence of KA platelets in the developed microbeads. The results of EDS spectra confirm the presence of KA in the polymeric microbeads. At pH 7.4 higher swelling degree and release rate were observed, suggesting that the developed microbeads might be suitable for intestinal drug delivery. The *in vitro* results were fitted into Peppas equation and the results showed that the drug mechanism followed a non-Fickian type of diffusion process. Based on the results, it was suggesting that Kaolin intercalated microbeads were potentially good carriers for the controlled release of CUR.

FUNDING

Nil

AUTHORS CONTRIBUTIONS

All the author has contributed equally.

CONFLICT OF INTERESTS

Declared none

REFERENCES

- Jain KK. Drug delivery systems-an overview. In: Drug delivery systems. Jain KK (Ed) Humana Press: Totowa, NJ; 2008. p. 1-50.

- Jones DS, Bruschi ML, de Freitas O, Gremião MPD, Lara EHG, Andrews GP. Rheological, mechanical and mucoadhesive properties of thermoresponsive, bioadhesive binary mixtures composed of poloxamer 407 and carbopol 974p designed as platforms for implantable drug delivery systems for use in the oral cavity. *Int J Pharm* 2009;372:49-58.
- Bruschi ML. 3-classification of therapeutic systems for drug delivery. In: Strategies to modify the drug release from pharmaceutical systems. Bruschi ML (Ed) Woodhead Publishing; 2015. p. 29-36.
- Reddy OS, Subha M, Jithendra T, Madhavi C, Rao KC. Fabrication of gelatin/karaya gum blend microspheres for the controlled release of distigmine bromide. *J Drug Delivery Ther* 2019;9:1-11.
- Ganguly S, Maity PP, Mondal S, Das P, Bhawal P, Dhara S, et al. Polysaccharide and poly(methacrylic acid) based biodegradable elastomeric biocompatible semi-iph hydrogel for controlled drug delivery. *Mater Sci Eng C* 2018;92:34-51.
- Sreekanth Reddy O, Subha MCS, Jithendra T, Madhavi C, Chowdoji Rao K. Curcumin encapsulated dual cross linked sodium alginate/montmorillonite polymeric composite beads for controlled drug delivery. *J Pharma Anal* 2020. <https://doi.org/10.1016/j.jpha.2020.07.002>
- Reddy OS, Subha M, Jithendra T, Madhavi C, Rao KC, Mallikarjuna B. Sodium alginate/gelatin microbeads-intercalated with kaolin nanoclay for emerging drug delivery in wilson's disease. *Int J Appl Pharm* 2019;11:71-80.
- Ngetich WK, Mwangi EM, Kiptoo J, Digo CA, Ombito JO. *In vitro* determination of sun protection factor on clays used for cosmetic purposes in kenya. *Chem Mater Res* 2014;6:25-30.
- Aguzzi C, Cerezo P, Viseras C, Caramella C. Use of clays as drug delivery systems: possibilities and limitations. *Appl Clay Sci* 2007;36:22-36.
- Viseras C, Cerezo P, Sanchez R, Salcedo I, Aguzzi C. Current challenges in clay minerals for drug delivery. *Appl Clay Sci* 2010;48:291-5.
- Rebello M, Viseras C, Lopez Galindo A, Rocha F, da Silva EF. Rheological and thermal characterization of peloids made of selected portuguese geological materials. *Appl Clay Sci* 2011;52:219-27.
- Silva HD, Pessoa-de-Souza MA, Fongaro G, Anunciação CE, Silveira Lacerda EdP, Barardi CRM, et al. Behaviour and recovery of human adenovirus from tropical sediment under simulated conditions. *Sci Total Environ* 2015;530:314-22.
- Vergaro V, Lvov YM, Leporatti S. Halloysite clay nanotubes for resveratrol delivery to cancer cells. *Macromol Biosci* 2012;12:1265-71.
- Williams LB. Geomimicry. Harnessing the antibacterial action of clays. *Clay Miner* 2017;52:1-24.
- Otto C, Haydel S. Microbicidal clays. Composition, activity, mechanism of action, and therapeutic applications. *Microbial pathogens and strategies for combating them. Sci Technol Education* 2013;2:1169-80.
- Misyak S, Burlaka A, Golotiuk V, Lukin S, Kornienko P. Antiradical, antimetastatic and antitumor activity of kaolin preparation "kremnevit". *Galician Med J* 2016;23:44-7.
- Pandey SP, Shukla T, Dhote VK, Mishra DK, Maheshwari R, Tekade RK. Use of polymers in controlled release of active agents. In: Basic fundamentals of drug delivery. Elsevier; 2019. p. 113-72.
- Obireddy SR, Chintha M, Kashayi CR, Venkata KRKS, Subbarao SMC. Gelatin-coated dual cross-linked sodium alginate/

- magnetite nanoparticle microbeads for controlled release of doxorubicin. *Chemistry Select* 2020;5:10276-84.
19. Calafiore R, Basta GPP, Montanucci P. Clinical grade sodium alginate for microencapsulation of myofibroblasts isolated from wharton jelly for prevention and treatment of autoimmune and inflammatory diseases. US Patent US20150290141A1; 2015.
 20. Mylangam CK, Beeravelli S, Medikonda J, Pidaparathi JS, Kolapalli VRM. Badam gum: a natural polymer in mucoadhesive drug delivery. Design, optimization, and biopharmaceutical evaluation of badam gum-based metoprolol succinate buccoadhesive tablets. *Drug Delivery* 2016;23:195-206.
 21. Meka VS, Nali SR, Songa AS, Kolapalli VRM. Characterization and *in vitro* drug release studies of a natural polysaccharide *terminalia catappa* gum (badam gum). *AAPS PharmSciTech* 2012;13:1451-64.
 22. Sadati Behbahani E, Ghaedi M, Abbaspour M, Rostamizadeh K, Dashtian K. Curcumin loaded nanostructured lipid carriers: *in vitro* digestion and release studies. *Polyhedron* 2019;164:113-22.
 23. Sun J, Bi C, Chan HM, Sun S, Zhang Q, Zheng Y. Curcumin-loaded solid lipid nanoparticles have prolonged *in vitro* antitumour activity, cellular uptake and improved *in vivo* bioavailability. *Colloids Surf B* 2013;111:367-75.
 24. Chen HW, Huang HC. Effect of curcumin on cell cycle progression and apoptosis in vascular smooth muscle cells. *Br J Pharmacol* 1998;124:1029-40.
 25. Reddy OS, Subha M, Jithendra T, Madhavi C, Rao KC. Emerging novel drug delivery system for control release of curcumin through sodium alginate/poly (ethylene glycol) semi ipn microbeads-intercalated with kaolin nanoclay. *J Drug Delivery Ther* 2019;9:324-33.
 26. Kar S, Kundu B, Reis RL, Sarkar R, Nandy P, Basu R, *et al.* Curcumin ameliorates the targeted delivery of methotrexate intercalated montmorillonite clay to cancer cells. *Eur J Pharm Sci* 2019;135:91-102.
 27. Costa P, Lobo JMS. Modeling and comparison of dissolution profiles. *Eur J Pharm Sci* 2001;13:123-33.
 28. Dash S, Murthy PN, Nath L, Chowdhury P. Kinetic modeling on drug release from controlled drug delivery systems. *Acta Pol Pharm* 2010;67:217-23.
 29. Gouda R, Baishya H, Qing Z. Application of mathematical models in drug release kinetics of carbidopa and levodopa er tablets. *J Dev Drugs* 2017;6:1-8.
 30. Dozie Nwachukwu SO, Danyuo Y, Obayemi JD, Odusanya OS, Malatesta K, Soboyejo WO. Extraction and encapsulation of prodigiosin in chitosan microspheres for targeted drug delivery. *Mater Sci Eng C* 2017;71:268-78.
 31. Arhewoh IM, Okhamafe AO. An overview of site-specific delivery of orally administered proteins/peptides and modelling considerations. *J Med Biomed Res* 2004;3:7-20.
 32. Rekik SB, Gassara S, Bouaziz J, Deratani A, Baklouti S. Development and characterization of porous membranes based on kaolin/chitosan composite. *Appl Clay Sci* 2017;143:1-9.
 33. Zhang Y, Long M, Huang P, Yang H, Chang S, Hu Y, *et al.* Intercalated 2d nanoclay for emerging drug delivery in cancer therapy. *Nano Res* 2017;10:2633-43.
 34. Jain S, Datta M. Montmorillonite-alginate microspheres as a delivery vehicle for oral extended release of venlafaxine hydrochloride. *J Drug Delivery Sci Technol* 2016;33:149-56.
 35. Jithendra T, Reddy OS, Subha MCS, Rao KC. Fabrication of drug delivery system for control release of curcumin, intercalated with magnetite nano particles through sodium alginate/polyvinylpyrrolidone-co-vinyl acetate semi ipn microbeads. *Int J Appl Pharm* 2020;12:249-57.
 36. Irfan Khan M, Khan HU, Azizli K, Sufian S, Man Z, Siyal AA, *et al.* The pyrolysis kinetics of the conversion of malaysian kaolin to metakaolin. *Appl Clay Sci* 2017;146:152-61.
 37. Reddy OS, Subha MCS, Mallikarjuna B, Madhavi C, Chowdoji Rao K. Fabrication of montmorillonite intercalated sodium alginate/poly (vinylpyrrolidone-co-vinyl acetate) beads for extended release of glycopyrrolate. *Ind J Adv Chem Sci* 2020;8:4-13.
 38. Govindaraju R, Karki R, Chandrashekarappa J, Santhanam M, Shankar AKK, Joshi HK, *et al.* Enhanced water dispersibility of curcumin encapsulated in alginate-polysorbate 80 nano particles and bioavailability in healthy human volunteers. *Pharm Nanotechnol* 2019;7:39-56.
 39. Madhavi C, Babu PK, Maruthi Y, Parandhama A, Reddy OS, Rao KC, *et al.* Sodium alginate-locust bean gum IPN hydrogel beads for the controlled delivery of nimesulide-anti-inflammatory drug. *Int J Pharm Pharm Sci* 2017;9:245-52.
 40. Chintla M, Obireddy SR, Areti P, Marata CSS, Kashayi CR, Rapoli JK. Sodium alginate/locust bean gum-g-methacrylic acid ipn hydrogels for "simvastatin" drug delivery. *J Dispersion Sci Technol* 2019;41:2192-202.